Selective Laser Melting: A Novel Method for Surface Roughness Analysis

Matej Babič[1,*] – Miha Kovačič[2,3,4] – Cristiano Fragassa[5] – Roman Šturm[2]

[1] Faculty of Information studies, Slovenia
[2] University of Ljubljana, Faculty of Mechanical Engineering, Slovenia
[3] Štore Steel, d.o.o., Slovenia
[4] College of Industrial Engineering, Slovenia
[5] University of Bologna, Department of Industrial Engineering, Italy

The present study introduces a novel approach to analyse the surface roughness of metal parts made by 3D selective laser melting (SLM). This technology, known for its ability to efficiently produce functional prototypes and limited-run series, is particularly effective when surface conditions directly meet usage requir ements. Thus, the suitability of surfaces is a critical factor, emphasizing the importance of new methods for predicting their quality. Here fractal geometry and network theory are integrated to delve into the complexities of SLM-produced surfaces, while machine learning and pattern recognition concepts are employed to evaluate the surface roughness. Specifically, genetic programming, artificial neural networks, support vector machine, random forest, k-nearest neighbors are compared in terms of accuracy demonstrating that only the first method provided valid estimation due to the presence of very little training data. Experimental work with EOS Maraging Steel MS1 and an EOS M 290 3D printer validates the method's practicality and effectiveness. Then, the research offers a fresh perspective in surface analysis and has significant implications for quality control in additive manufacturing, potentially enhancing the precision and efficiency of 3D metal printing.

Keywords: additive manufacturing, selective laser melting, surface roughness, fractal geometry, network theory, genetic programming

Highlights
- *Introduces a novel method combining fractal geometry and network theory to analyse surface roughness.*
- *Employs techniques like machine learning and pattern recognition for accurate surface characterization.*
- *Offers a direct comparison of predictions made by genetic programming and other predictive algorithms.*
- *Demonstrates practical applications of these methods to the case of Metal Laser Melting.*
- *Details experimental work using EOS Maraging Steel MS1 and an EOS M 290 3D printer.*
- *Presents a comprehensive analysis, proving the efficiency of the proposed method.*
- *Offers significant implications for improving quality control and precision in 3D metal printing industries.*

0 INTRODUCTION

Additive manufacturing (AM) [1], also known as three-dimensional (3D) printing, is a production technology able to create three-dimensional objects by adding successive layers of material, unlike traditional manufacturing techniques, such as milling or turning, which remove material. This process relies on digital models to guide the deposition of material, enabling the creation of complex geometries that are difficult or impossible to achieve with conventional methods. Moreover, it allows for an effective solution of production especially in the case prototypes and small series.

At the same time, AM convenience and wider adoption as definitive process technology are currently limited by aspects such as the surface quality of the final products [2]. This quality represents a crucial aspect in the case of industrial goods due to its significant impact on their key characteristics. Surface roughness, in fact, directly affects aesthetic appeal, mechanical performance, and operational efficiency of products, as it influences essential characteristics such as wear, fatigue, and corrosion resistances. It also plays a vital role in determining the conditions of interfacing, which can be critical in many applications.

Achieving a comprehensive understanding of surface roughness is challenging due to the multitude of processing factors involved such as:
- the complexity of surface textures requires sophisticated metrics and analysis techniques to be fully considered, especially on a microscale.
- different materials and manufacturing processes produce a wide variety of surface characteristics, making standardization of measurement methods difficult.
- environmental and operational factors can alter surface conditions over time, necessitating continuous or repeated analysis.

The integration of this sort of knowledge into practical procedures and methods needs

---

*Corr. Author's Address: Faculty of Information studies, Novo mesto, Slovenia, babicster@gmail.com

313

interdisciplinary expertise, combining material science, engineering, and data analysis.

Then, there is a growing attention for more effective and powerful tools, able to analyse and predict surface characteristics, also involving concepts of artificial intelligence (AI). This is the exact baseline for the present study that merges fractal geometry and network theory to recognize surface distinctive patterns and machine learning (ML) methods for their investigation [3].

Beginning with the fundamental definition of the most relevant aspects of the current study:

- ML [4] refers to a large variety of mathematical, statistical, and computational methods able to solve a problem not directly, but by searching for patterns inside input data. The solution is calculated not according to a clear formula but exploiting dependences. The more data such a model processes and the longer it is used, the more accurate the results become.

- Pattern recognition [5] is a discipline whose goal is to classify 'objects' into categories or classes, based on the analysis and interpretation of their images, utilizing techniques from fields such as ML, statistics, and data analysis.

- Fractal, as a term, was coined by Benoit Mandelbrot [6] to describe an uncommon group of mathematical objects that played a significant role in the transition from classical to modern mathematics. Classical mathematics, rooted in Euclidean geometry and Newton's dynamics, gave way to modern mathematics with the introduction of new concepts like the Cantor set theory and the space-filling Peano curve. These new mathematical structures represent the vast possibilities within pure mathematics. Among other uses, fractals demonstrated to be highly valuable in characterizing image complexity inside engineering applications.

- Graph theory [7] is a branch of discrete mathematics that investigates the properties of graphs. In a general sense, a graph is represented as a set of vertices (nodes) connected by edges and arcs.

- Network theory [8], inside this broad framework, extends the concepts of the graph theory to the analysis of real-world networks and systems.

These general concepts, strictly related to the AI application to the solution of engineering problems, have been here used for assessing the surface quality in components fabricated by selective laser melting (SLM).

SLM [9] is one of the most common AM processes in the case of metals and metallic alloys, falling, then, within the broader family of production methods for successive stratifications. A laser beam selectively melts metal powder particles to create, layer by layer, the part. During the procedure, the laser beam acts on the surface of the component being built, forming a melting pool on it. In the meantime, metal powder enters the processing chamber from a nozzle which, again due to the effect of the beam, passes into a liquid state, thus mixing with the melting bath. After cooling, solid connecting structures form between the original material and the added one, little different from those created by traditional casting processes. Then, SLM does not sinter the powders but melts them into a homogeneous mass making possible to create parts with flexibility, speed, and quality, also assuring high and stable material properties.

Fig. 1 shows the SLM general operating scheme and its main systems such as:

- the construction chamber, i.e. the controlled environment where sintering takes place.
- the construction bed, i.e. the surface on which the object is built.
- the tank with the powder to be sintered.
- the recoater blade which distributes the powder evenly over the build bed.
- the laser that melts the powder to form the layers of the object.
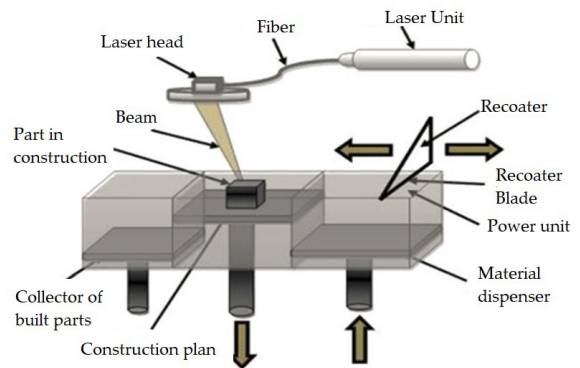- the laser beam and recoater blade movement control system.

Fig. 1. *Simplified diagram of the SLM process*

1 MATERIALS AND METHODS

1.1 Equipment and Technology

The EOS M 290 SLM machine has been used [10], Fig. 2. The wide range of usable materials, a comprehensive monitoring suite, and easy integration

into the production steps make this machine the proper choice for flexible series production of metal parts.

Fig. 2. *EOS M290 system used for SLM* **[10]** *SIEVA 3D Lab*

In the SLM, the surface quality is strictly related to the technology. In the working process, a directed laser beam acts on the workpiece, forming a melt pool on it. Here it turns into a liquid state, providing a connection with the source material. After cooling, connecting rollers or structures of a certain configuration and size, or even completely new parts, are formed on the surface. The average thickness of one layer is 0.1 mm. A jet of protective gas, predominantly argon, is also supplied to the processing zone for improving the process. The optical unit of the machine, under the control of the software package, moves itself along the part, drawing edges and lines. The uniform layer thickness is ensured by a system of built-in touch sensors.

In terms of physical and mechanical properties, products obtained by the SLM method are superior, in general, to classical analogues. Since metal powders are not sintered, but melted under the influence of laser radiation, until a homogeneous mass is formed, which, after cooling, retains the specified geometry, then the structure is homogeneous, non-porous, which has a positive effect on the strength of the finished product. The printed products are characterized by high dimensional accuracy. Its surface requires virtually no finishing treatment (which also saves both time and money).

1.2 Digital Procedure

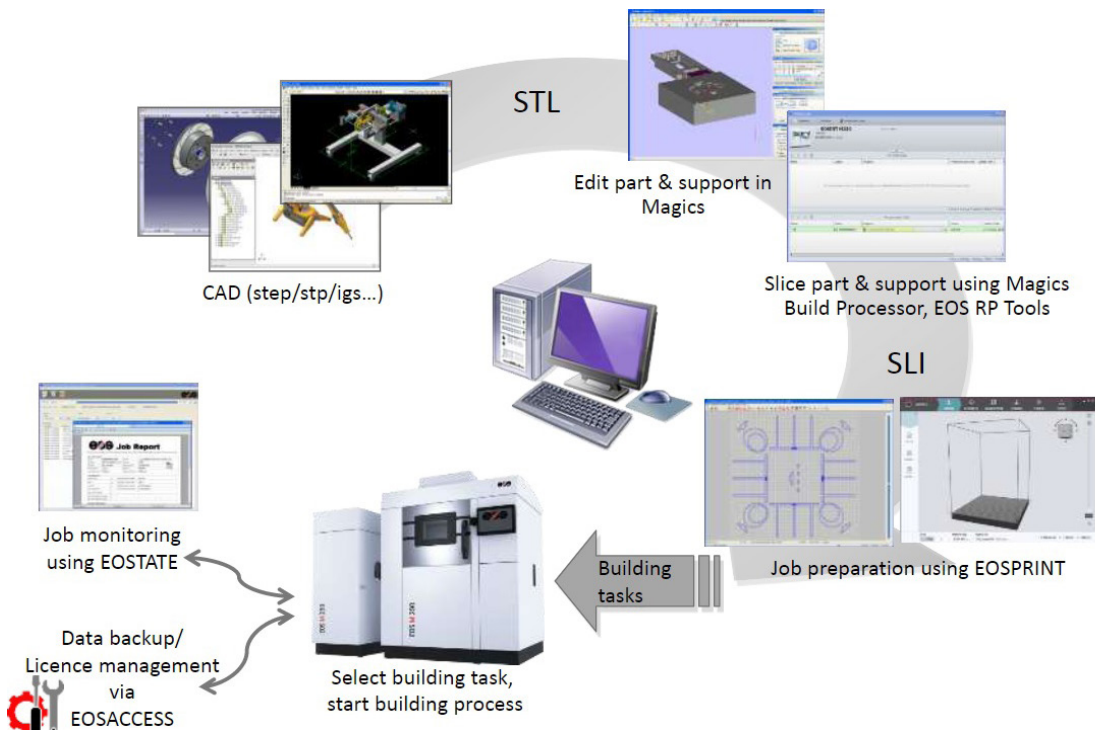According to the SLM process, three main steps have been implemented (Fig. 3):

Fig. 3. *Procedure for production of parts by SLM [10]*

1. Preparation: once a CAD model is created, it is transferred to specialized printer software. At the same stage, the material is selected and the position of the components relative to each other on the construction substrate is specified. This integrated approach permits to minimize material consumption, reduce the cost of money and time for the production process. Based on the information received, the machine program independently selects exposure vectors and process speed, laser beam power, the distance between the dashed lines that determine the processing step, the layer thickness (since the program conditionally breaks the object into separate layers).

2. Printing process: the equipment prints the product layer by layer, repeating the operations cyclically. A thin layer of powder is fed into the work area. It is also filled with an inert gas, often argon, nitrogen (oxygen content is minimal). Its particles, under the influence of laser radiation, are soldered to those parts of the surface that are included in the computer model. As soon as one layer is printed, the working platform will automatically lower to its thickness (30 mm to 50 mm) and the technological process will be repeated again. Thus, layer by layer in height, the finished part is synthesized.

3. Post-processing: at this stage, the working powder, which was not involved in the technological process, is removed from the construction chamber by a vacuum block with a stream of air. It is sifted and can be reused. Next, the specialist manually removes the supporting elements that were installed inside the flow channel for better fixation of the product. All irregularities are sanded down. The final stage is finishing turning.

1.3 Material Preparation

EOS Maraging Steel MS1 has been chosen as material. It is a tool steel powder intended for processing on EOS DMLSTM systems. This kind of steel is characterized by having very good mechanical properties and being easily heat-treatable using a simple thermal age-hardening process to obtain excellent hardness and strength. Parts built in this material have a chemical composition following US classification 18 % Ni Maraging 300, European 1.2709 and German X3NiCoMoTi 18-9-5. Moreover, the parts are machinable after the manufacturing process and can be easily post-hardened to more than

50 HRC by age-hardening at 490 °C (914 °F) for 6 hours. In both as-built and age-hardened states these parts can be machined, spark-eroded, welded, micro shot-peened, polished and coated if required. Due to the layerwise building method, the parts have a certain anisotropy, which can be reduced or removed by appropriate heat treatment – e.g. solution treatment at 940 °C for 2 hours.

In the case, twenty cubic specimens, with length 10 mm, have been made by SLM and investigated in terms of surface quality.

As first, a profilometer has permitted to measure roughness surface. Contact profilometry is a quantitative technique known to reflect the irregularities of the surface profile of metal materials, including SLM parts [11]. The most common parameter derived by profilometry is the average roughness (Ra), for quantifying the surface texture and ensuring quality control in manufacturing processes. It commonly helps in assessing and predicting mechanical performance and evaluating the overall aesthetic appearance of the finished products. In the case, Ra has been detected along x- and y-axes, namely Ra_x and Ra_y.

Then, a microstructural analysis has been performed on all specimens. Microstructures are shown in Fig. 4, limited to some representative cases (i.e., specimens id. 3, 11, 14, 18 and 19).

Physical characteristics including strength, toughness, ductility, hardness, corrosion and wear resistance, etc., are all significantly influenced by a material's microstructure. These characteristics control, in turn, when and how materials can be used in industrial applications. At the same time, as also evident in Fig. 4, microstructures are quite complex to be analysed. The present investigation assumes that the fractal geometry, differently respect to the classical Euclidean geometry, can help in characterizing such complexity.

1.4 Fractals

In fractal geometry two aspects deserve special attentions:
1. Self-similarity / self-affinity
2. Fractal dimension.

1.4.1 Self-Similarity and Self-Affinity

These concepts can be defined using the mathematical notion of iterative function system (IFS) [12], proposed by Hutchinson [13]. A self-similar set, E,
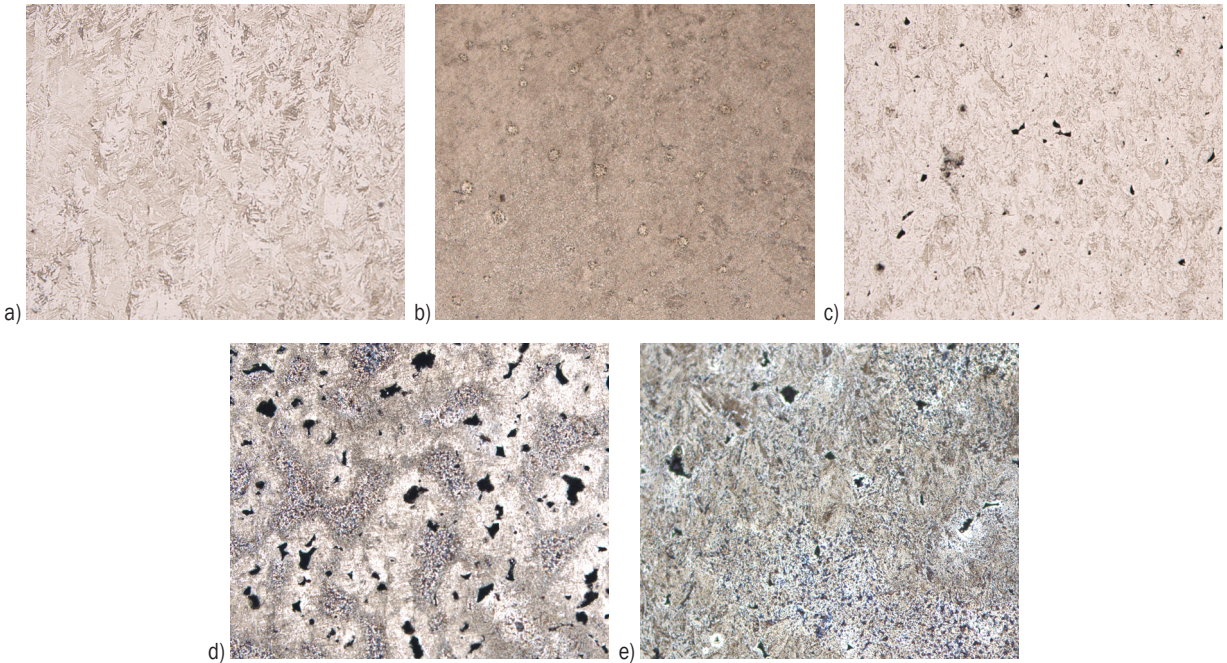
Fig. 4. *Representative microstructures under investigation; a) Id. 3, b) Id. 11, c) Id. 14d and Id. 18at 50×, and e) ; and Id. 19 at 100×*

can be infinite or finite copies of itself (Fig. 6) and expressed as

$$E = \bigcup_{i=1}^{m} f_i(E), \qquad (1)$$

where E is the invariant set or attractor of the IFS, f_i is the transformation function describing the relationship between the invariant set and the constituent parts.

Two objects are said to be self-similar if one is a union of a (limited) number of smaller similar copies of itself. The transformation function f_i defines a scalar transformation reducing its size and the shifting of origin inside E. Here f_1 defines the top-left shift and f_2 defines the bottom-right shift. Difference between self-similar and self-affine transformation present in Fig. 5.

Self-affinity including self-similar geometry can be classified into three groups [14]: exactly self-affine, quasi self-affine and statistically self-affine (Fig. 7).
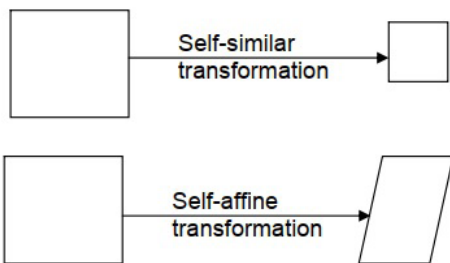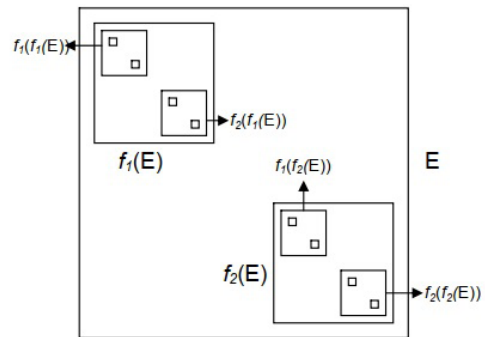
Fig. 6. *Construction of the invariant set E*

Fig. 7. *Types of self-affinity: a) exactly self-affine, b) quasi self-affine, and c) statistically self-affine*

1.4.2 Fractal Dimension

The fractal dimension (FD) is a common term invoked in geometry to provide a rational statistical index of complexity detail in a pattern. It quantifies how the detail of the pattern changes with the scale at which it is measured. It can be particularly useful for analysing images, as it provides a way to characterize irregular

Fig. 5. *Self-similar and self-affine transformation*

and complex structures, offering insights into patterns and textures within the image
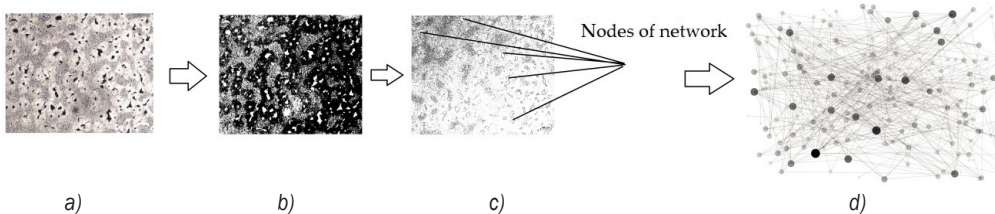
1.4.3 Image Processing

The probability density function (PDF) of black/white image has been here used as main concept for image processing and to establish FD of microstructure [15], as represented in Fig. 8.
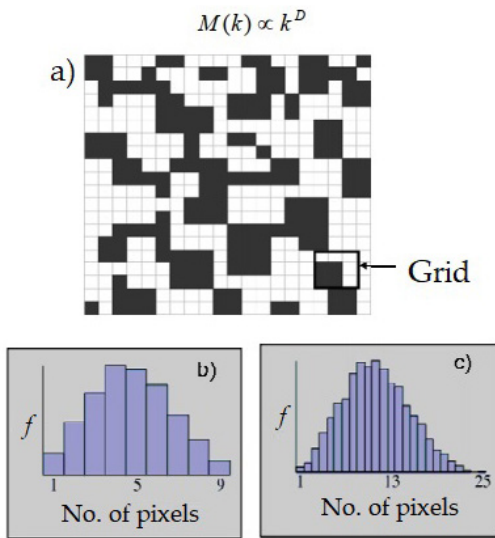
Fig. 8. *Probability-density function; a) pixel map (black regions), showing a representative 3×3 sliding grid for which the count, N(k) = 4, b) frequency distribution of pixel counts for a 3×3 window, and c) frequency distribution of pixel counts for a 5×5 window*

A square grid of size ($k \times k$) is slid over the image from left to right, top to bottom by shifting its position by one pixel from its previous one. Let $N(k)$ be the number of black pixels at a particular position of the square grid where $N(k) \leq k^2$. The first order moment, $M(k)$, of the probability density function $P(k)$ of the $N(k)$ values for different positions of the square grid can be derived by using the following formula.

$$M(k) = \sum_{i=1}^{N(k)} i \cdot P_i(k) \quad \text{where} \quad \sum_{i=1}^{N(k)} P_i(k) = 1. \quad (2)$$

$M(k)$ is often termed the 'mass dimension'. The relationship between the first order moment value $M(k)$ and k may be given by

$$M(k) \propto k^D. \quad (3)$$

1.5 Pattern Recognition

A novel method for pattern recognition (PR) utilizing graph theory has been established here, following the next rules. The collection of nodes $V(u, v)$ and the set of edges $E(u, v)$ constitute the graph $G = (V, E)$. First, graphs (networks) have been created using microstructures (one graph per each microstructure). White island nodes have been generated by detecting SLM in photos of 3D printing materials. Then, a network has been constructed by connecting the neighbors of the closest node.

Fig. 9 provides a quick representation of the four main phases characterizing this new procedure for pattern recognition by the network theory.

It is worth noting that the network of nodes represents the microstructure on one hand, while on the other hand, it can be described using typical parameters from network theory.

Among others, the network density (η) is here of special interest. It can be defined as the fraction of edges present over all possible edges and represented as:

$$\eta = 2 \cdot E / V \cdot (V - 1), \quad (4)$$

where V is the number of vertexes, and E is the number of edges in the network.

1.6 Modelling

With the scope of modelling roughness surface, similarly to other past investigations [16] to [19], two AI-based approaches have been here used: genetic programming (GP) and neural network (NN).

Fig. 9. *A new method for pattern recognition by using network theory*

1.6.1 Genetic Programming

The GP is an automatic procedure to create or modify programs using genetic-based algorithms [20]. With it, programs are 'grown' to increasingly solve the given computational problem more effectively, according to a certain fitness function for the chromosomes. In GP, the individuals in a population represent programs. These programs are conveniently represented as symbolic trees, where functions are depicted by internal nodes, and sub-trees are attached as input parameters. The leaves of such a tree represent constants, task input parameters, or program directive commands (as in Fig. 10):

$$\left(68 + \left(\frac{Y}{9}\right)\right) - \left(5 * \cos(X)\right)$$
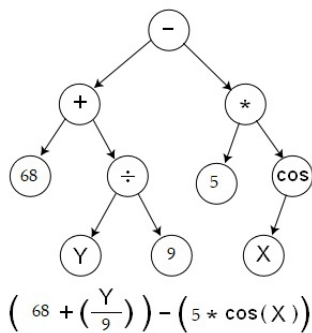
Fig. 10. *Simple tree program in GP*

a)   b)
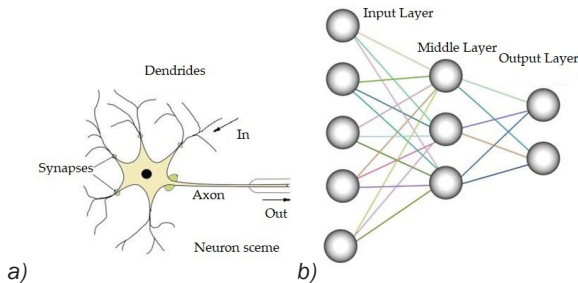
Fig. 11. *Comparison between neural network structures: a) natural network; b) artificial network*

1.6.2 Neural Network

The NN is a methodological procedure derived from research into the human brain, then applied to a loosely coupled family of models characterized by a large parametric space and flexible structure [21]. Most new models have been developed for non-biological applications, although many associated terms reflect their origins. A NN is a massively parallel distributed processor that has the natural ability to store empirical information and make it available for use. It is like the brain in two ways: knowledge is acquired by the network through the learning process. To store knowledge, interneuron connections of varying strengths, called synaptic weights, are used, thus creating a parallel between biological and artificial structures in the way of processing information (Fig. 11).

2 RESULTS AND DISCUSION

The present investigation has involved 17 specimens made by SLM, each one characterized by a specific combination of process parameters, i.e. laser beam power (P), from 170 W to 320 W, and speed (v), from 700 mm/s to 1300 mm/s. Actually, although 20 SLM combinations (of laser speed and power) have been initially considered, at high power density, i.e. low scan speed and high laser power, the surface poor quality has been immediately evident, suggesting removing these specimens, consequently reduced to 17.

From each specimen ($S1, S2, …, S17$), a micrograph has been detected and then analysed using the fractal dimension (FD) and network density (η), dimensionless parameters.

Table 1 in the Appendix A reports results from this analysis, also including the average values of roughness Ra_x and Ra_y (in µm), as measured with the contact profilometry.

About the range assumed by the roughness, it is possible to note that the:

- lowest Ra_x (= 5.06 µm) has been achieved using a laser scan with power P = 170 W and speed v = 1000 mm/s (specimen S15).
- highest Ra_x (= 7.19 µm) with 270 W and 1150 mm/s (specimen S6).
- lowest Ra_y (= 4.90 µm) with 270 W and 1000 mm/s (specimen S5).
- highest Ra_y (= 6.96 µm) for 220 W and 1300 mm/s (specimen S12).

Furthermore, in general:

- the roughness Ra_y is very similar for all laser parameters, ranging between 5.7µm and 6.2 µm.
- an evident tendency of reducing roughness emerges only when the laser power is increased to 320 W.
- when evaluating roughness in the x direction, the lowest surface roughness is achieved with the lowest laser power of 170 W and at low laser scan speeds between 700 mm/s and 1000 mm/s.
- low surface roughness can be achieved at a high laser power of 320 W and with a higher laser scan speed of 1300 mm/s, which is beyond the current experimental setup.

Figs. 12 and 13 can offer a quick overview of the available results. In the four representations of Fig. 12, e.g., the variation of fractal dimension (FD), network density (η) and average roughness (Ra_x and Ra_y) with power (P) and speed (v) of the laser beam is shown. In Fig. 13, the Ra_x and Ra_y dependences from v at different P are detailed.

First, it can be seen that the measurements uniformly cover the entire range of variability of the process parameters considered (P and v). At the same time, no significant relationship between the parameters seems to emerge at first sight.

Even a linear correlation analysis (CA), with calculation of the Spearman coefficient (ρ), does not reveal strong correlations between the data. The most significative correlations trends to each other are, e.g., P and FD which show a negative correlation in average intensity ($\rho = -0.417$) or the positive correlation of P with R_y, R_x, η ($\rho = 0.388$, 0.369 and 0.361, respectively). Other weak correlations are also present, such as, i.e., the relation of v with Ra_x and FD ($\rho = 0.323$, -0.325).

In general, it is possible to state that already under these conditions (few data) the presence of correlations between the parameters emerges, but without the possibility to take them into account through a linear approach. It therefore becomes essential to use more advanced tools.
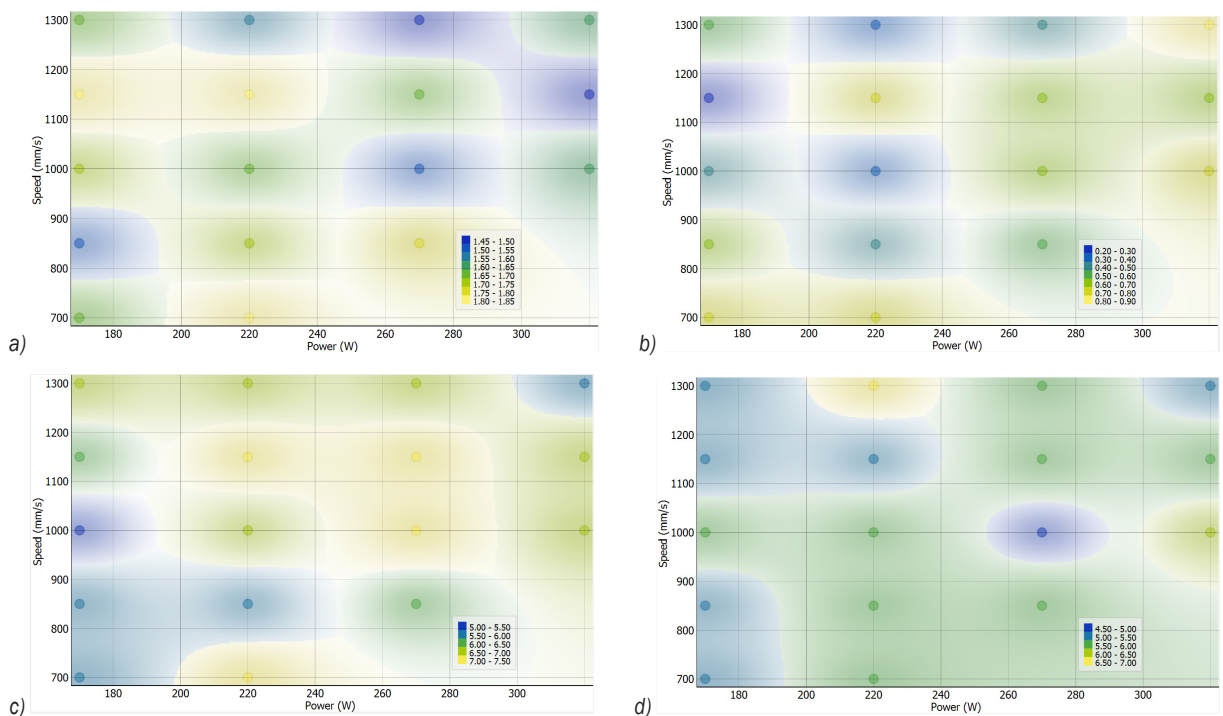

Fig. 12. *Overview of data variations in terms of: a) fractal dimension (FD), b) network density (η), c) average roughness along X-axis (Ra_x), and (d) Y-axis (Ra_y) as the power and translation speed of the laser beam vary*
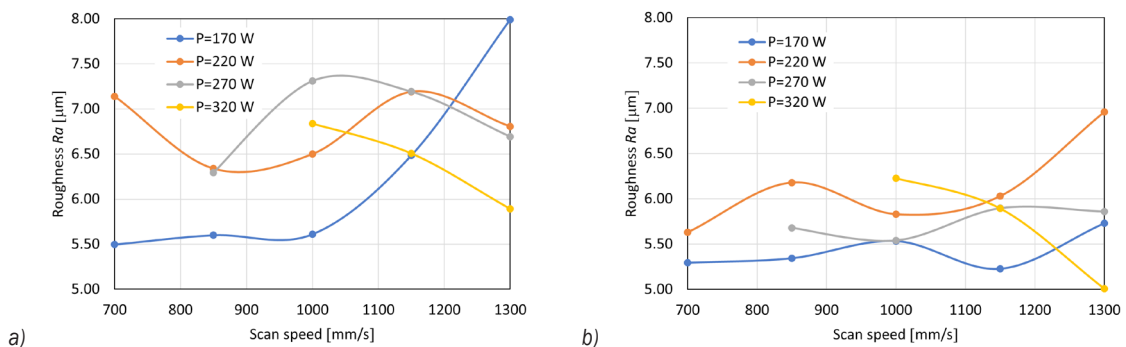

Fig. 13. *Relationship roughness (Ra) vs laser speed (v) at different power (P): a) Ra_x; b) Ra_y*

Then, referring to the same specimens $(S1, S2, …, S17)$, Table 2 in Appendix B presents the predicted values of average roughness (Ra_x and Ra_y), as obtained by GP and NN predictors through a (non-linear) ML approach. The study has been done by the orange data mining (ver. 3.35.0), a data analysis platform developed by the University of Ljubljana, Slovenia and widely used for scientific applications.

Specifically, given the limited consistency of the data sample, a 'cross-validation' approach was preferred as learning method. In this system, a single item is eliminated from the dataset and used to verify the validity of the predictions, while all other items are used to train the ML system. This operation is repeated for each item in the dataset (extracting a different item for each step), and the overall results are obtained by combining the partial outcomes.

Measured and predicted values from Tables 1 and 2, respectively, can then be compared. In particular, while Fig. 13 presents a specimen-by-specimen comparison of predicted vs. measured Ra_x and Ra_y, Fig. 14 provides a quick overview of the GP and NN accuracy in estimating surface roughness. In the figure, this accuracy can be assessed by considering

the distance of the points from the bisector of the axes: the closer a point is, the greater the estimation precision. In fact, while the expected (experimental) values are reported on the abscissa, those predicted by MF methods on the ordinate, where the proximity of the points to the dotted bisector indicates the accuracy. Fig. 15 present accuracy of GP and NN methods in estimating surface roughness for Ra_x and Ra_y.

It immediately emerges that the GP model, as detailed in Appendix B, in almost all cases, is able to predict the expected values with very high precision, rated at 97.6 % for Ra_x and 98.2 % for Ra_y in terms of as mean squared error (MSE) or .923 and .931 as Pearson correlation coefficient.

In practical terms, these results demonstrate that there is at least one ML technique capable of mathematically managing the complexity of the problem under consideration. They also confirm the possibility of predicting the microstructure of an SLM process a priori, even in the presence of little data on which to base the predictive model. Furthermore, although these results have been validated in the specific case of surface roughness, there are no reasons to believe that it is not possible to extend the
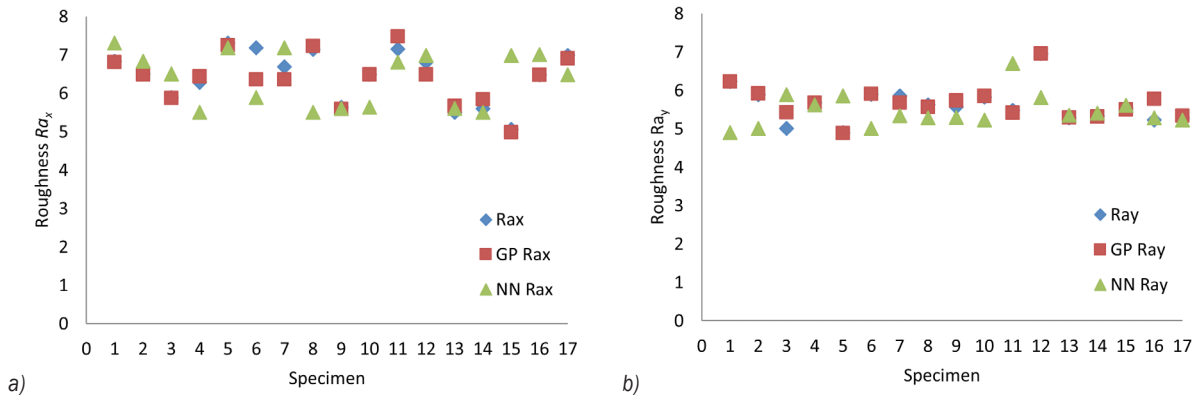

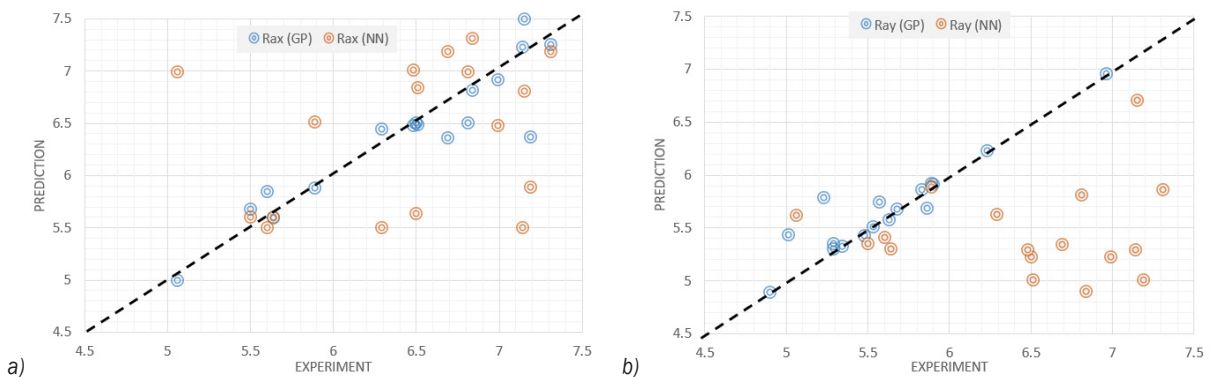**Fig. 14.** *Roughness estimation by GP and NN: a) Ra_x; b) Ra_y*

Fig. 15. *Accuracy of GP and NN methods in estimating surface roughness: a) Ra_x; b) Ra_y*

method to the study of other properties attributable to it.

3 CONCLUSIONS

The present research introduces a new method that integrates fractals, network theory and genetic programming with the scope of analysing the surface roughness of metal additive parts. Specifically, it is focused on SLM and uses EOS Maraging Steel MS1 processed by an EOS M 290 3D printer. Findings demonstrate a significant potential in predicting the surface roughness when the GP is used. But, much more importantly, they demonstrate that the combined application of fractal geometry and machine learning methods can significantly enhance our understanding of the complexities involved in the surface analysis.

Thus, this study not only contributes to the field of additive manufacturing by offering a more efficient and precise approach to quality control but also sets the stage for future explorations into other materials and refining analytical techniques. The potential of the proposed method in supporting the 3D metal printing practices is substantial, indicating a promising future for the industry in terms of both innovation and application.

4 NOMENCLATURES

R^2 R-Squared, [-]
Ra Roughness (average), [μm]
Ra_x, Ra_y Roughness (average) along x, y, [μm]
η network density, [-]

5 REFERENCES

[1] Frazier, W.E. (2014). Metal additive manufacturing: A review. *Journal of Materials Engineering and Performance*, vol. 23, p. 1917-1928, **DOI:10.1007/s11665-014-0958-z**.

[2] Gockel, J., Sheridan, L., Koerper, B., Whip, B. (2019). The influence of additive manufacturing processing parameters on surface roughness and fatigue life. *International Journal of Fatigue*, vol. 124, p. 380-388, **DOI:10.1016/j.ijfatigue.2019.03.025**.

[3] Rodríguez, G.G., Gonzalez-Cava, J.M., Pérez, J.A.M. (2020). An intelligent decision support system for production planning based on machine learning. *Journal of Intelligent Manufacturing*, vol. 31, p. 1257–1273, **DOI:10.1007/s10845-019-01510-y**.

[4] Lee, J.H., Shin, J., Realff, M.J. (2018). Machine learning: Overview of the recent progresses and implications for the process systems engineering field. *Computers & Chemical Engineering*, vol. 114, p. 111-121, **DOI:10.1016/j.compchemeng.2017.10.008**.

[5] Anil, K.J., Duin, R..P.W., Jianchang, M.M. (2000). Statistical pattern recognition: a review. *IEEE Transactions on Pattern Analysis and Machine Intelligence*, vol. 22, no. 1, p. 4-37, **DOI:10.1109/34.824819**.

[6] Mandelbrot, B. (1977). *Fractals*. Freeman, San Francisco.

[7] Bondy, J.A., Murty, U.S.R. (2008). *Graph Theory*. Springer, New York, **DOI:10.1007/978-1-84628-970-5**.

[8] Chen, W.-K. (1997). *Graph Theory and Its Engineering Applications*, Vol. 5. World Scientific, **DOI:10.1142/2446**.

[9] Torres-Carrillo, S., Siller, H.R., Vila, C., López, C., Rodríguez, C.A. (2020). Environmental analysis of selective laser melting in the manufacturing of aeronautical turbine blades. *Journal of Cleaner Production*, vol. 246, 119068, **DOI:10.1016/j.jclepro.2019.119068**.

[10] EOS (2024). from https://www.eos.info/de, accessed on 2024-04-01.

[11] ASME B46.1-2009. *Surface Texture: Surface Roughness, Waviness, and Lay*. American Society of Mechanical Engineers, Society of Automotive Engineers, New York.

[12] Brasil, J.E., Oliveira, E.R., Souza, R.R. (2023). Thermodynamic formalism for general iterated function systems with measures. *Qualitative Theory of Dynamical Systems*, vol. 22, 19, **DOI:10.1007/s12346-022-00722-7**.

[13] Hutchinson, J.E. (1981) Fractals and Self-similarity. *Indiana University Mathematical Journal*, vol. 30, no. 5, p. 713-747, **DOI:10.1512/iumj.1981.30.30055**.

[14] Bral, S., Dyga, R. (2021). Self-affinity approach for the determination of flow regime in pipelines. *Measurement*, vol. 168, 108452, **DOI:10.1016/j.measurement.2020.108452**.

[15] Joyce, D. (2014). *Axioms of Probability*. Clark University. Worcester.

[16] Babic, M., Calì, M., Nazarenko, I., Fragassa, C., Ekinovic, S., Mihaliková, M., Janjić, M., Belič, I. (2018). Surface roughness evaluation in hardened materials by pattern recognition using network theory. *International Journal on Interactive Design and Manufacturing*, vol. 13, p. 211-219, **DOI:10.1007/s12008-018-0507-3**.

[17] Fragassa, C., Babic, M., Pavlovic, A., do Santos E.D. (2020) Machine learning approaches to predict the hardness of cast iron. Tribology in Industry, vol. 42, no. 1, p. 1-9, **DOI:10.24874/ti.2020.42.01.01**.

[18] Babic, M., Fragassa, C., Lesiuk, G., Marinkovic, D. (2020) New method for complexity determination by using fractals and its applications in material surface characteristic. *International Journal for Quality Research*, vol. 14, no. 3, p. 705-716, **DOI:10.24874/IJQR14.03-04**.

[19] Babic, M., Wangyao, P., Ster, B., Marinković D., Fragassa C.. (2022). Modelling the surface roughness of steel after laser hardening by using 2D visibility network, convolutional neural networks and genetic programming. *FME Transactions*, vol. 50, no. 3, p. 393-402, **DOI:10.24874/IJQR14.03-04**.

[20] Koza, J.R. (1992). Genetic Programming: On the Programming of Computers by Means of Natural Selection, MIT, Press Cambridge, Cambridge.

[21] Hardesty, L. (2017). *Explained: Neural network*s. MIT News Office, from https://news.mit.edu/2017/explained-neural-networks-deep-learning-0414, accessed on 2022-06-02.

6 APPENDIX A

Table 1. *Data from SLM specimens*

Specimen	Laser Beam		Microstructure		Roughness	
	P [W]	v [mm/s]	FD [-]	η [-]	Ra_x [µm]	Ra_y [µm]
S1	320	1000	1.62	0.74	6.84	6.23
S2	320	1150	1.49	0.68	6.51	5.89
S3	320	1300	1.65	0.89	5.89	5.01
S4	270	850	1.78	0.52	6.29	5.68
S5	270	1000	1.55	0.61	7.31	4.90
S6	270	1150	1.67	0.65	7.19	5.90
S7	270	1300	1.47	0.42	6.69	5.86
S8	220	700	1.83	0.78	7.14	5.63
S9	220	850	1.74	0.42	5.64	5.57
S10	220	1000	1.66	0.35	6.50	5.83
S11	220	1150	1.86	0.74	7.15	5.48
S12	220	1300	1.59	0.32	6.81	6.96
S13	170	700	1.68	0.73	5.50	5.29
S14	170	850	1.51	0.65	5.60	5.34
S15	170	1000	1.72	0.43	5.06	5.53
S16	170	1150	1.83	0.29	6.48	5.23
S17	170	1300	1.69	0.59	6.99	5.29
GP parameters	X1	X2	X3	X4	Y1	Y2

Table 2. *Prediction roughness Ra_x and Ra_y by GP and NN*

Specimen	GP Rax	GP Ray	NN Rax	NN Ray
S1	6.81	6.23	7.31	4.90
S2	6.49	5.92	6.84	5.01
S3	5.88	5.43	6.51	5.89
S4	6.44	5.68	5.50	5.63
S5	7.25	4.89	7.19	5.86
S6	6.36	5.91	5.89	5.01
S7	6.36	5.68	7.19	5.34
S8	7.23	5.57	5.50	5.29
S9	5.59	5.74	5.60	5.30
S10	6.50	5.86	5.64	5.23
S11	7.49	5.42	6.81	6.71
S12	6.50	6.96	6.99	5.81
S13	5.67	5.30	5.60	5.35
S14	5.85	5.32	5.50	5.41
S15	4.99	5.51	6.99	5.62
S16	6.48	5.78	7.01	5.29
S17	6.91	5.34	6.48	5.23

7 APPENDIX B

Genetic Programming (GP) model for roughness estimation

$$
\begin{aligned}
Ra_x = 5.21662 - \frac{1}{X1-X2}\Bigg(&X1 + X3X4 + \frac{X3}{-6.85234 + 0.854064X3 + 6.85234X4 + X4^3} + \frac{X3X4}{-6.85234 + 0.854064X3 + 6.85234X4 + X4^3} \\[4pt]
&+ \frac{X3}{-6.85234 + 1.70813X3 + 6.85234X4 + \frac{6.85234X4^2(0.854064X3 + X3X4)}{X1 - X3X4^2}} \\[4pt]
&- \frac{13.7047 + X1 - 0.854064X3 - \frac{X1-X3}{X3X4^2} - 6.85234X4 + \frac{X1 - \frac{X1-X3}{-1+X3}}{0.145936X3 + \frac{X3}{X4} + 6.85234X4^2}}{6.85234X4 + \dfrac{X3}{-X1 + 0.854064X3 - \frac{0.145936\left(X1 - \frac{X1-X3}{-1+X3}\right)}{X4} + 5.85234X4 + \frac{X3}{0.145936X3 + 6.85234X4^2}}} \\[4pt]
&- X4\Bigg(X1X4 + \frac{X1 - X3 - \frac{0.145936\left(-\frac{X1-X3}{-1+X3} + X1X4\right)}{X4^2}}{6.85234X4 + \frac{X3}{-6.85234 + 0.854064X3 + 7.85234X4}} \\[4pt]
&- \frac{1.17087\left(X1 - 1.85406X3 - \frac{X1X4^2(0.854064X3 + X3X4)}{X1 - X3X4^2}\right)}{X3}\Bigg)\Bigg)
\end{aligned}
\tag{3}
$$

$$
\begin{aligned}
Ra_y = \; & 6.32887 + \left(7.1054X4 + \frac{-0.77653 + \dfrac{X3X4}{\dfrac{X3X4}{3.77194 - 3.77194X4} - X3X4^2}}{X3} \right) \\[2em]
& \Bigg/ \left(3.74432 - X1 - 1.28778X3 + 0.265116X2X4 + \frac{7.1054 + \dfrac{-0.77653 + \dfrac{X3X4}{\dfrac{X3X4}{3.77194 - 3.77194X4} - X3X4^2}}{X3}}{4.54847 - \dfrac{X3}{X4}} \right) \\[2em]
& + \frac{1}{X1}\left(0.164639\left(-0.77653 + \frac{7.07391X4(3.77194 - X3X4)}{-X3X4 + \dfrac{X3X4}{3.77194 - 3.77194X4}} \right) \right) \\[2em]
& + \frac{X1 - X4}{3.74432 + \dfrac{-0.77653 + \dfrac{X2}{2X1X3} + 0.859262X3 + 0.265116X3X4}{0.77653 - 0.164639X2X4 + 0.265116X2X4^2} + \dfrac{7.1054 + \dfrac{7.07391X4}{X3} - \dfrac{0.77653X3X4^2}{3.77194 - X4^2}}{-6.85044 - X1 + 0.265116X2 + \dfrac{X3}{X2}}} \\[2em]
& + \frac{7.1054X4 + \dfrac{-0.77653 + \dfrac{X3X4}{\dfrac{X3X4}{3.77194 - 3.77194X4} - X3X4^2}}{X3}}{0.77653 - \dfrac{X3}{X1} + 0.265116X3X4 - \dfrac{-0.77653 + \dfrac{X3X4}{\dfrac{X3X4}{3.77194 - 3.77194X4} - X3X4^2}}{X3X4}}
\end{aligned} \tag{4}
$$

where $X1 = P$ [W], $X2 = v$ [mm/s], $X3 = FD$, and $X4 = \eta$.